# Development of PWSCC Initiation Model for Alloy 182 Welds Considering Thermal Aging and Cold Work Effects

Jae Phil Park [a], Seung Chang Yoo [b], Ji Hyun Kim [b], Chi Bum Bahn [a*]
[a]*School of Mechanical Engineering, Pusan National University, Busan 46241, Republic of Korea*
[b]*School of Mechanical, Aerospace and Nuclear Engineering, Ulsan National Institute of Science and Technology, Ulsan 44919, Republic of Korea*
[*]*Corresponding author: bahn@pusan.ac.kr*

## 1. Introduction

Over the past few decades, initiation of primary water stress corrosion cracking (PWSCC) of Alloy 182 welds has been one of the most critical safety issues in nuclear power plants (NPPs) [1]. Therefore, it is crucial to predict the initiation of PWSCC under a given condition of components. Owing to the long-term operation of existing NPPs, it becomes also important to consider the effect of thermal aging on PWSCC initiation. Furthermore, cold work is another important process that can significantly alter the mechanical properties, microstructures, and PWSCC resistance of Ni-based alloys [2].

In this context, we experimentally investigated the effects of thermal aging and cold work on the microstructure, mechanical properties, and PWSCC initiation of Alloy 182 welds. Furthermore, we developed a PWSCC initiation model based on the plastic energy concept which can consider the thermal aging and cold work effects. The PWSCC initiation data used for the model development included not only the experimental data from this work but also data from published reports considering censored data.

## 2. Methods and Results

### *2.1 Preparation of test specimens*

The Alloy 182 weld deposit was prepared on a 316L stainless steel (SS) plate using shielded metal arc welding. The welding current, voltage, and speed ranges were 140–150 A, 25–28 V, and 15–18 cm/min, respectively. Table 1 shows the chemical composition of the Alloy 182 weld.

Table 1. Chemical composition of Alloy 182 weld

| C | Si | Mn | P | S | Fe |
|---|---|---|---|---|---|
| 0.048 | 0.08 | 8.38 | 0.011 | 0.007 | 3.10 |
| **Cu** | **Ni** | **Ti** | **Cr** | **Cb+Ta** | |
| 0.01 | REM. | 0.02 | 13.97 | 1.29 | |

After welding, the fabricated weld deposit was divided into four parts to assign different post-processing as follows:

- No post-processing, as-welded (AW)
- Heat treatment equivalent to 15 years of thermal aging during plant operation (15Y)
- Heat treatment equivalent to 30 years of thermal aging during plant operation (30Y)
- Cold work via cold rolling with 20% thickness reduction (CR)

The plant operation temperature was assumed to be 320 °C. To simulate the 15Y and 30Y thermal aging conditions, we conducted accelerated heat treatment at 400 °C under an argon environment for 1713 h and 3427 h, respectively.

For cold work processing, five steps of cold rolling were carried out to achieve a 20% thickness reduction after cutting the Alloy 182 portion from the 316L SS base plate. After post-processing, specimens for microstructural analyses and tensile and PWSCC tests were cut using electrical discharge machining along the T-L direction [3].

### *2.2 Microstructural analysis*

We focused on the precipitates along grain boundaries because the PWSCC in Alloy 182 welds is an intergranular phenomenon [4]. It was observed that the amount and size (i.e., area fraction) of the precipitates increased with thermal aging. However, cold work had no noticeable effect on the precipitate fraction. We found that the precipitates along grain boundaries were Cr carbides ($Cr_{23}C_6$ or $Cr_7C_3$), which is consistent with precedent research on similar materials [5]. The coarsened grain boundary precipitates, which were formed during thermal aging, were primarily composed of Cr carbides. This is apparent because the amount and diffusion rates of other minor elements (such as Nb and Ti) were relatively low at 400 °C.

We performed the first-order kernel average misorientation (KAM) images analysis, which are closely related to the residual strain or dislocation density. It is observed that cold work increases the value of KAM, in particular, near the grain boundaries, implying the accumulation of geometrically necessary dislocation [48]. On the contrary, thermal aging decreases the overall KAM value. Therefore, it is concluded that cold work increases localized residual strain and thermal aging relieves existing residual strain formed during the welding process.

### *2.3 Tensile test*

The tensile tests were performed according to the ASTM E8/E8M standard at both room temperature (RT) and 325 °C. During these tests, the tensile displacement rate was constantly maintained at 0.63 mm/min. A total of 45 specimens were fabricated following the standard rod-type design in the ASTM E8/E8M; however, the specimen size was proportionally reduced because of the limited size of the weld deposit.

Table 2. Measured mean mechanical properties of Alloy 182.

| Specimen Condition | | CR | AW | 15Y | 30Y |
|---|---|---|---|---|---|
| YS [MPa] | RT | 711.8 | 425.0 | 421.7 | 412.9 |
| | 325 °C | 628.8 | 370.7 | 347.1 | 321.9 |
| UTS [MPa] | RT | 795.9 | 603.2 | 631.1 | 636.0 |
| | 325 °C | 724.5 | 561.8 | 554.7 | 530.8 |
| Uniform Elongation (uEL) [%] | RT | 8.00 | 27.61 | 34.99 | 39.23 |
| | 325 °C | 10.23 | 34.43 | 37.08 | 34.63 |

Table 2 summarizes the measured mechanical properties. At RT, it is shown that cold work increases both yield strength (YS) and ultimate tensile strength (UTS) but decreases elongation. On the contrary, thermal aging increases UTS and elongation. At the elevated temperature of 325 °C, cold work increases both YS and UTS but decreases elongation, like the trend at RT. However, thermal aging decreases YS, UTS, and also elongation (30Y) at 325 °C, unlike the trend at RT.

### *2.4 PWSCC initiation test and modeling*

The size of the as-machined PWSCC testing specimen was 10 mm × 100 mm × 3 mm. Subsequently, the specimens were deformed to have a U-bend shape, according to the ASTM G30 standard. Figure 1 illustrates the schematic of the fabricated U-bend specimens. The specimens were loaded and constrained using the Inconel alloy X-750 high-strength spring to mitigate stress relaxation at the elevated testing temperature. Other components that could contact the Alloy 182 U-bend were composed of Alloy 600 to prevent galvanic corrosion. A total of 46 (AW: 16 ea., 15Y/30Y/CR: 10 ea. each) U-bend specimens were fabricated and tested under the simulated primary water condition of the pressurized water reactor (PWR) with the testing temperature of 340 °C, autoclave pressure of 16 MPa, dissolved oxygen of less than 5 ppb, dissolved hydrogen of 30 cc/kg $H_2O$, and Li and B concentrations of 1200 ppm and 2 ppm, respectively. During the PWSCC test, the U-bend specimens were periodically retrieved from the autoclave to identify the occurrence of PWSCC. In this work, the criterion of crack initiation was whether or not a crack is visible through naked eyes.

For a more realistic estimate of the applied stress/strain in the U-bend specimens, a commercial finite element analysis (FEA) software ABAQUS (Ver. 2016) was used. The input material properties for plastic stress–strain data were obtained from the tensile test results. Other input properties such as elastic modulus, Poisson's ratio, and temperature-dependent thermal expansion coefficient were obtained from published data of Alloy 600 [6]. The FEA was conducted via the following two steps: 1) U-bending at room temperature using rigid rollers and 2) increasing the specimen temperature to 325 °C.

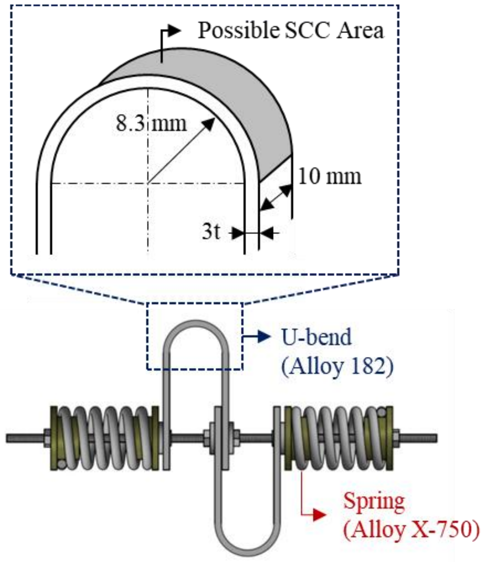


Fig. 1. Schematic of U-bend specimen for PWSCC initiation test.

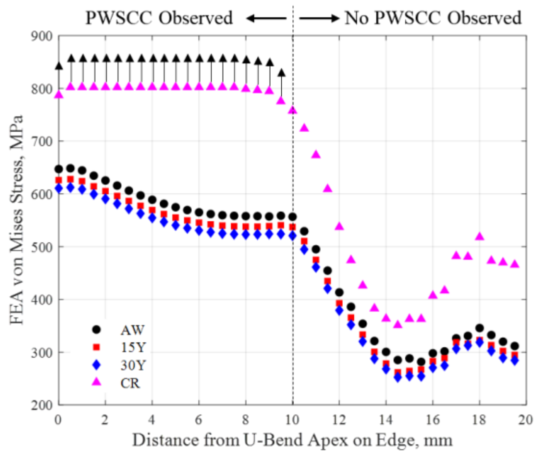


Fig. 2. Result of U-bend stress estimation by FEA.

Figure 2 shows the estimation results of the U-bend stress via FEA. Because the applied stress in the U-bend specimens is not uniaxial, the von Mises effective stress is represented and used in this study. It is shown that the stress applied to the CR specimen is the highest and that to the 30Y specimen is the lowest. However, it should be noted that the plotted stress of the CR specimen is only the lower bound because the calculated equivalent plastic strain (i.e., PEEQ) during the FEA exceeded the measured uniform elongation.

Figure 3 shows the example images of PWSCC initiation and propagation. As shown in this figure, it was difficult to identify the occurrence of cracking until the crack was sufficiently wide because of the uneven specimen surface. The minimum length of the identifiable crack through the naked eyes was approximately 2 mm. It was observed that the average propagation speed of CR specimens was considerably higher than that of the other specimens.

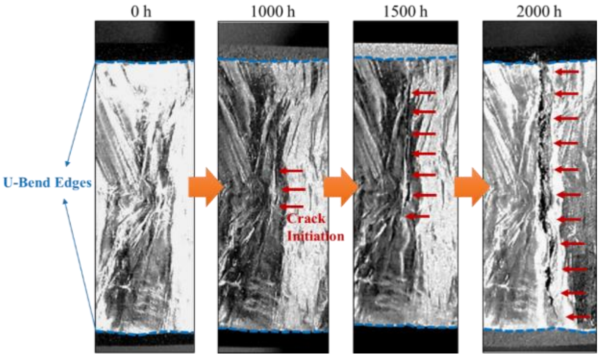


Fig. 3. PWSCC initiation and propagation of #13-AW specimen.

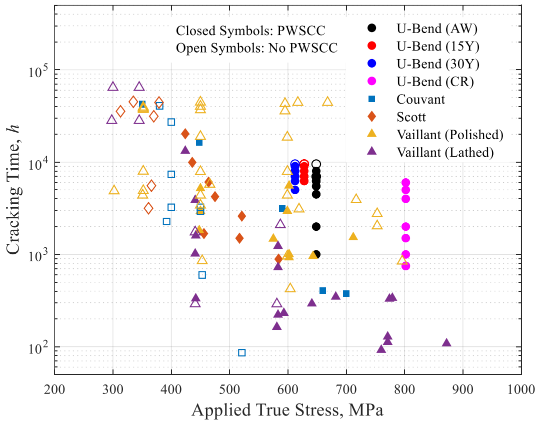


Fig. 4. All Alloy 182 PWSCC initiation data including U-bend and published data (corrected at 340 °C).

Table 3. Information of published PWSCC initiation data sets of Alloy 182.

| Data Reference | YS [MPa] | | UTS [MPa] | | PWSCC Specimen | Number of Data |
|---|---|---|---|---|---|---|
| Couvant [7] | RT<br>350 °C | 386<br>347 | RT<br>350 °C | 627<br>568 | Tensile | 6 SCC<br>9 No SCC |
| Scott [8] | RT<br>350 °C | 363<br>321.7 | RT<br>350 °C | 637<br>549.3 | Pressurized Capsule | 8 SCC<br>6 No SCC |
| Vaillant [9-11] | RT<br>350 °C | 395<br>353 | RT<br>350 °C | 657<br>584 | Tensile (Polished) | 10 SCC<br>30 No SCC |
| | | | | | Tensile (Lathed) | 18 SCC<br>8 No SCC |

Figure 4 shows all PWSCC initiation data, including those from this study and the published data (see Table 3). We only collected the published Alloy 182 PWSCC initiation data for which the applied stress, YS, and UTS were known [7-11]. The plotted data points of previous reports were extracted through graph digitizing. The effect of different testing temperatures used in the published data was normalized at 340 °C using the Arrhenius equation with the activation energy of 185 kJ/mol. The U-bend data plotted using the closed symbols in Fig. 4 indicate the observation time of cracking (not the precise cracking time but the upper limit). The applied stresses of the U-bend data were assumed to be the highest FEA stresses in Fig. 2. Although this assumption may not be accurate for CR specimens, it is a conservative assumption considering the resulting PWSCC initiation model.

Because of the large scattered and censored PWSCC initiation data, a probabilistic approach was used. We modeled the PWSCC initiation time based on the 2-parameter Weibull distribution. To consider the effects of thermal aging and cold work, a new factor of plastic energy ratio ($r_{\mathrm{PE}}$) was adopted. The followings are the model proposed in this work:

$$F(t;\beta,\eta) = 1 - \exp\left[-\left(\frac{t}{\eta}\right)^{\beta}\right] \tag{1a}$$

where

$$\eta = \lambda(r_{\mathrm{PE}})^{-m} \tag{1b}$$

$$r_{\mathrm{PE}} = \frac{\sigma^2 - \sigma_{\mathrm{th}}^2}{\sigma_u^2 - \sigma_{\mathrm{th}}^2} \tag{1c}$$

$$\sigma_u = \mathrm{UTS}_{\mathrm{ET}}(1 + \mathrm{uEL}_{\mathrm{ET}}) \tag{1d}$$

$$\mathrm{uEL}_{\mathrm{ET}} = a_0(\mathrm{UTS}_{\mathrm{ET}} - \mathrm{YS}_{\mathrm{ET}})^{b_0} + \frac{\mathrm{UTS}_{\mathrm{ET}}}{E_{\mathrm{ET}}} \tag{1e}$$

$F$ is the cumulative distribution function (CDF), $t$ is the time, and $\beta$ and $\eta$ are the shape and scale parameters of the Weibull distribution, respectively. $\sigma$ is the applied true stress, $\sigma_{\mathrm{th}}$ is a yield stress when the material is perfectly annealed and there is no damage, $\sigma_u$ is the true stresses at the start of necking (or plastic instability), and $E$ is the elastic modulus of the material. $\lambda$ is the calibration parameter which included the effects of temperature, water chemistry, specimen geometry/size, surface finish, criterion of crack initiation, and so on. Therefore, the estimates of $\lambda$ varied with each data set. We also assumed that the estimates of the Weibull shape parameter $\beta$ varied with each data set. The subscript ET indicates the elevated temperature range under the typical PWR primary water condition (e.g., 325–350 °C); uEL is the uniform (engineering) elongation, and $a_0$ and $b_0$ are the material-dependent fitting parameters. In the case of Alloy 182, we estimated the fitting parameters using the tensile test data from this study. The estimated fitting parameters for Alloy 182 were $a_0$ = 7.725×10$^{-5}$ MPa$^{-1}$ and $b_0$ = 1.570.

To consider the censored data, we used the probabilistic method of maximum likelihood estimation [12] to estimate parameters. The estimation objective is to find four parameter estimates ($\beta, \lambda, \sigma_{\mathrm{th}}$, and $m$) using the data in Figs. 4 and Tables 2 and 3 with four input variables ($\sigma, E_{\mathrm{ET}}, \mathrm{YS}_{\mathrm{ET}}$, and $\mathrm{UTS}_{\mathrm{ET}}$). In this study, the estimates were numerically calculated.

Table 4 shows the estimation results and Fig. 5 presents a correlation of the measured PWSCC initiation time and the predicted PWSCC initiation time. We represented the median of the distribution (i.e., the time at which the probability of cracking was 50%) as the predicted PWSCC initiation time. The black dashed lines in Fig. 5 indicate the shifted 1:1 prediction lines with a factor of five. When comparing the results, it should be noted that a model becomes more plausible when the NO PWSCC (i.e., censored) data are located as far above as possible from the 1:1 prediction line, contrary to the ordinary PWSCC data. Therefore, it can be concluded that the estimated model well fits the raw data.

Table 4. Estimation result of Alloy 182 PWSCC initiation model.

| Models | | PER-Power Model |
|---|---|---|
| Input Variables | | $\sigma, E_{ET}, YS_{ET}, UTS_{ET}$ |
| Output Variable | | $F(t)$ |
| Log-Likelihood | | -490.61 |
| Parameters depending on Data Set | U-Bend (All) | $\beta$ = 2.246, $\lambda$ = 3194 h |
| | Couvant | $\beta$ = 1.533, $\lambda$ = 326 h |
| | Scott | $\beta$ = 2.851, $\lambda$ = 231 h |
| | Vaillant (Polished) | $\beta$ = 0.513, $\lambda$ = 8256 h |
| | Vaillant (Lathed) | $\beta$ = 1.219, $\lambda$ = 122 h |
| Universal Parameters regardless of Data Set | | $\sigma_{th}$ = 298 MPa<br>$m$ = 2.41 |

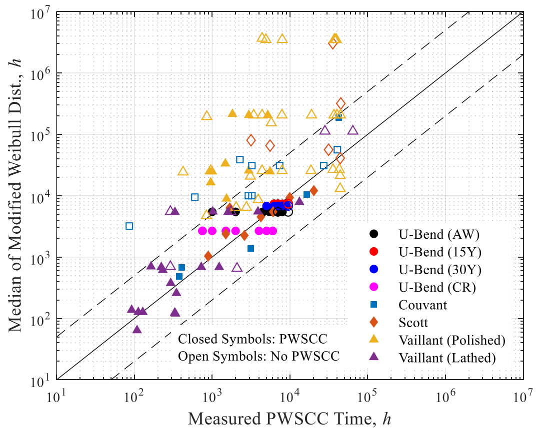


Fig. 5. Correlation of measured PWSCC initiation time versus predicted PWSCC initiation time for Alloy 182.

### 3. Conclusions

We experimentally investigated the effects of thermal aging and cold work on the microstructure, mechanical properties, and PWSCC initiation of Alloy 182 welds. Furthermore, we developed a probabilistic PWSCC initiation model for Alloy 182 considering thermal aging and cold work. Based on the results, it was estimated that the PWSCC resistance of the Alloy 182 weld increases and decreases with thermal aging time when the applied stress is maintained constantly.

### Acknowledgement

This work was supported by the Korea Institute of Nuclear Safety (KINS) and Nuclear Safety Research Program through the Korea Foundation Of Nuclear Safety (KoFONS) using the financial resource granted by the Nuclear Safety and Security Commission (NSSC) of the Republic of Korea. (No. 1403006). This work was also supported by the "Human Resources Program in Energy Technology" of the Korea Institute of Energy Technology Evaluation and Planning (KETEP), granted financial resource from the Ministry of Trade, Industry & Energy, Republic of Korea. (No. 20184010201660)

### REFERENCES

[1] P. Scott, M.C. Meunier, Materials reliability program: review of stress corrosion cracking of alloys 182 and 82 in PWR primary water service (MRP-220), EPRI Palo Alto CA. 1015427 (2007).

[2] T. Maeguchi, K. Sakima, K. Sato, K. Fujimoto, Y. Nagoshi, K. Tsutsumi, PWSCC Susceptibility of Alloy 690, 52 and 152, in: Proceedings of the 18th International Conference on Environmental Degradation of Materials in Nuclear Power Systems–Water Reactors, Springer, 2019: pp. 485–500.

[3] P. Scott, Experimental Program on the Effects of Surface Condition on Primary Water Stress Corrosion Cracking of Alloy 182 Welds, (2007).

[4] Y.S. Lim, S.S. Hwang, S.W. Kim, H.P. Kim, Primary water stress corrosion cracking behavior of an Alloy 600/182 weld, Corrosion Science. 100 (2015) 12–22.

[5] Y.S. Lim, H.P. Kim, H.D. Cho, H.H. Lee, Microscopic examination of an Alloy 600/182 weld, Materials Characterization. 60 (2009) 1496–1506.

[6] Special Metals, INCONEL Alloy 600, (n.d.). https://www.specialmetals.com/assets/smc/documents/alloys/inconel/inconel-alloy-600.pdf (accessed June 20, 2020).

[7] T. Couvant, F. Vaillant, Initiation of PWSCC of weld Alloy 182, in: Proceedings of the 15th International Conference on Environmental Degradation of Materials in Nuclear Power Systems—Water Reactors, Springer, 2011: pp. 1141–1154.

[8] P. Scott, M. Foucault, B. Brugier, J. Hickling, A. McIlree, Examination of stress corrosion cracks in Alloy 182 weld metal after exposure to PWR primary water, in: Proceedings of the 12th International Conference on Environmental Degradation of Materials in Nuclear Power System–Water Reactors–Edited by TR Allen, PJ King, and L. Nelson TMS (The Minerals, Metals & Materials Society), 2005: pp. 497–509.

[9] F. Vaillant, J.-M. Boursier, T. Couvant, C. Amzallag, J. Champredonde, Influence of a cyclic loading on the initiation and propagation of PWSCC in weld metal 182, in: 12th Int. Conf. on Environmental Degradation of Materials in Nuclear Power Systems-Water Reactors, Snowbird, UA, 2005: pp. 14–18.

[10] G. Troyer, S. Fyfitch, K. Schmitt, G. White, C. Harrington, Dissimilar metal weld PWSCC initiation model refinement for xLPR part I: a survey of alloy 82/182/132 crack initiation literature, in: Proceedings of the 17th International Conference on Environmental Degradation of Materials in Nuclear Power Systems—Water Reactors, Ottawa, ON, Canada, 2015: pp. 9–13.

[11] F. Vaillant, J.-M. Boursier, C. Amzallag, C. Bibollet, S. Pons, Environmental behaviour and weldability of Ni-base weld metals in PWRs, Revue Générale Nucléaire. (2007) 62–71.

[12] J.P. Park, S. Mohanty, C.B. Bahn, S. Majumdar, K. Natesan, Weibull and Bootstrap-Based Data-Analytics Framework for Fatigue Life Prognosis of the Pressurized Water Nuclear Reactor Component Under Harsh Reactor Coolant Environment, Journal of Nondestructive Evaluation, Diagnostics and Prognostics of Engineering Systems. 3 (2020).